PAPER

Check for updates

Shielding against breast tumor relapse with an autologous chemo-photo-immune active Nano–Micro-Sera based fibrin implant†

Mimansa,[a] Mohammad Adeel Zafar,[b] Dinesh Kumar Verma,[c] Reena Das,[d] Javed Naim Agrewala [b] [b] and Asifkhan Shanavas [b] *[a]

Local recurrence post-surgery in early-stage triple-negative breast cancer is a major challenge. To control the regrowth of a residual tumor, we have developed an autologous therapeutic hybrid fibrin glue for intra-operative implantation. Using autologous serum proteins as stabilizers, we have optimized high drug-loaded lapatinib-NanoSera (Lap-NS; ~66% L.C.) and imiquimod-MicroSera (IMQ-MS; ~92% L.C.). Additionally, plasmonic nanosera (PNS) with an ~67% photothermal conversion efficiency under 980 nm laser irradiation was also developed. While localized monotherapy with either Lap-NS or PNS reduced the tumor regrowth rate, their combination with IMQ-MS amplified the effect of immunogenic cell death with a high level of tumor infiltration by immune cells at the surgical site. The localized combination immunotherapy with a Nano–MicroSera based hybrid fibrin implant showed superior tumor inhibition and survival with significant promise for clinical translation.

1. Introduction

Surveillance, Epidemiology and End Results reports suggest that 10–15% of women suffer from triple-negative breast cancer (TNBC), the most aggressive of all sub-types where receptors of oestrogen, progesterone and human epidermal growth factor 2 (HER-2) are absent, thereby making the condition therapeutically most challenging. Surgery is a primary frontline intervention for breast cancer patients despite being a majorly invasive procedure.[1,2] However, TNBC bears heightened risk of relapse after surgical resection, primarily attributable to its invasive characteristics, limited treatment modalities, and dismal prognosis.[3–5] To overcome these challenges, conventional treatments such as chemotherapy, radiation, and immunotherapy can be seamlessly integrated as adjuvant therapies following surgery, for prolonged and enhanced therapeutic outcomes.[6] While chemotherapy conventionally utilizes systemic and oral administration routes, the implementation of regional and loca-

lized delivery of active pharmaceutical ingredients (APIs) has emerged as a strategy to mitigate dose-limited toxicity. This approach has spurred the development of drug-loaded oncological implants such as Gliadel®, Oncogel™, and Sinofuan®, leveraging biodegradable polymers for sustained release.[7–9] Local implants for delivering chemotherapeutic drugs and radiation at the surgical bed can bestow less frequent dosing, site specific delivery, improved compliance, less side effects and patient convenience.[10,11] While existing commercially available implants rely on synthetic polymers, approaches utilizing biomaterials of endogenous origin, such as fibrin glue, offer multifaceted applications. They are adaptable in clinical settings as both a haemostat and an adhesive sealant, showcasing versatility beyond their traditional synthetic counterparts.[12]

Nanotechnological tools hold promise for mitigating the toxicity and enhancing the solubility of chemotherapeutics. However, their progress is hindered by challenges such as poor tumor bioavailability (less than 0.7% of the injected dose) and rapid clearance by the reticuloendothelial system (RES), leading to a deceleration in their development.[13] Localized implantation of nanoparticles with fibrin glue enables immediate bioavailability at the target site, controlled release and perioperative penetration of the cargo with enhanced immunotherapeutic outcomes.[14] Intraoperative application of fibrin glue is also promising to treat locally advanced TNBC where the possibility and convergence of multiple treatment modalities might achieve superior efficacy and improve the quality of life of patients by toning down systemic exposure to adjuvant therapies. Despite the availability of commercial
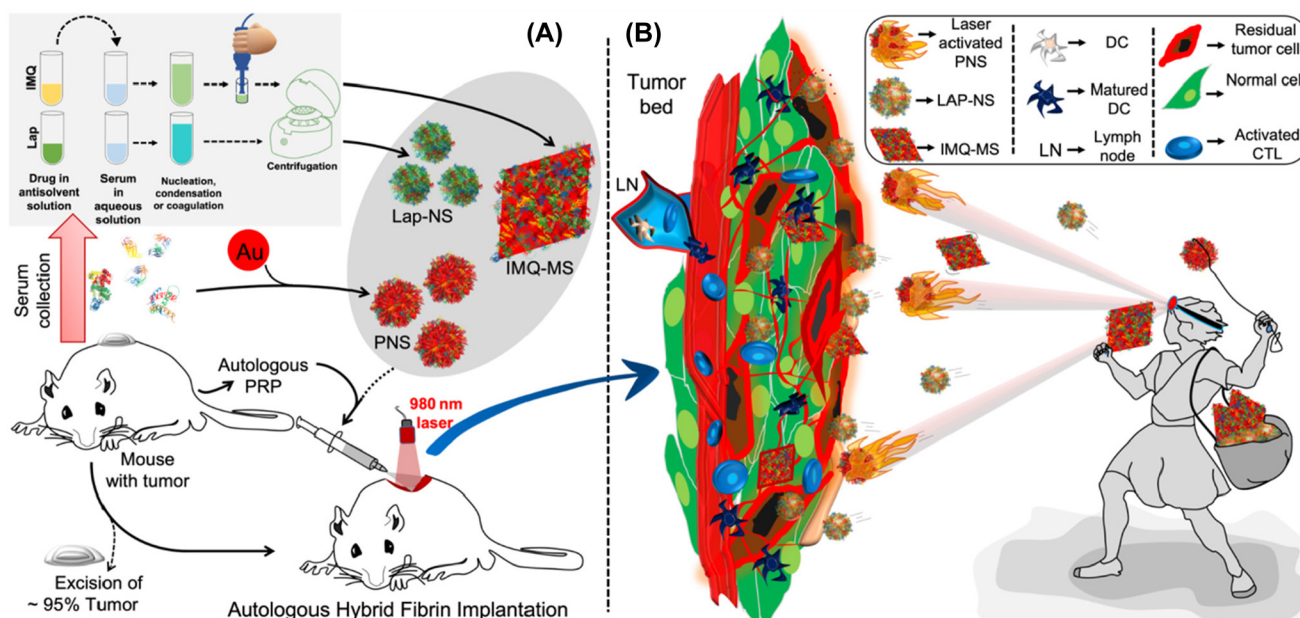
[a]*Inorganic & Organic Nanomedicine (ION) Lab, Chemical Biology Unit, Institute of Nano Science and Technology, Sector-81, Knowledge City, Sahibzada Ajit Singh Nagar, Punjab 140306, India. E-mail: asifkhan@inst.ac.in*
[b]*Department of Biomedical Engineering, Indian Institute of Technology Ropar, Rupnagar, Punjab 140001, India*
[c]*All India Institute of Medical Sciences Bilaspur, Changar Palasiyan, Noa, Himachal Pradesh, 174001, India*
[d]*Department of Haematology, Post Graduate Institute of Medical Education and Research (PGIMER), Chandigarh 160012, India*
†Electronic supplementary information (ESI) available. See DOI: https://doi.org/10.1039/d4nr01076k

Fig. 1 (A) Work flow for the preparation of Nano–MicroSera (NMS) and its application at the tumor bed with platelet rich plasma based fibrin glue using the all-in-one autologous strategy; (B) the hybrid fibrin glue initiates concurrent chemo-photothermal attack on residual cancer cells and further activation of immune cells.

fibrin glue, clinicians are leaning towards autologous platelet rich plasma-based fibrin glue for ophthalmological, cartilage repair, and maxillofacial surgery among many as a more innocuous, cost-effective option.[15–17]

Although various nano-drug delivery systems, including liposomes, polymers, proteins, and silica, have undergone extensive exploration, a persistent challenge lies in achieving optimal loading efficiency. This issue arises from the predominant possession of the nanoparticle volume by the carrier matrix.[18] Recently our group showed that API nanocrystals stabilized with autologous serum proteins with high drug loading (>60% w/w) termed 'NanoSera'.[19] Furthermore, we have demonstrated the stabilization of photo-active metal nanoparticles with autologous serum proteins with confirmed safety in mouse models.[20,21] Building on previous reports, an 'all-in-one' autologous therapeutic strategy has been formulated, emphasizing the predominant utilization of host-derived biomaterials in the development of a hybrid fibrin glue. This innovative hybrid fibrin glue is investigated for its localized application, incorporating a combination of 'Nano–MicroSera' containing lapatinib, gold nanodendrites, and imiquimod. Our aim was to explore this integrated approach for the chemo-photothermal immunotherapeutic management of residual TNBC post-resection (Fig. 1).

2. Materials and methods

2.1 Synthesis and characterization

Lapatinib-NanoSera. A microcentrifuge tube (MCT) with 20 µL of 10 mg mL^{-1} lapatinib prepared in DMSO added to

480 µL of water was mixed with 17.5 µL of human serum in 482.5 µL of water. It was mixed gently and centrifuged at 5000 rpm for 5 min. The supernatant was separated and absorbance was recorded to measure the amount of unentrapped drug and the pellet was redispersed in aqueous medium appropriate for further experimentation.

PNS. PNS synthesis was followed up from our previous work.[20] A one-pot synthesis was carried out in a MCT, in which different components such as 400 µL of 5 mM HauCl$_4$, 80 µL of 10 mg ml^{-1} fetal bovine serum (FBS) or human serum or mouse serum (MS), 65 µL of 100 mM NaOH and then 300 µL of 100 mM ascorbic acid were added in series. The volume was made up to 1000 µL with water and centrifuged at 5000 rpm for 5 min. The supernatant was discarded and the pellet was redispersed into water followed by sonication until complete redispersion.

Imiquimod-MicroSera. Briefly, 1 mg mL^{-1} of imiquimod (IMQ) stock was prepared in DMSO and heated at 80 °C until it completely dissolved. Next, 400 µL of this IMQ stock was mixed with 100 µL of water and immediately added to a MCT containing 27.5 µL of serum mixed with 472.5 µL of water and homogenized (T-10 basic ULTRA-TURRAX®) at 7100 rpm for 30 seconds. The sample was then centrifuged at 5000 rpm for 5 min. The supernatant was separated and absorbance was recorded to calculate the amount of unentrapped drug and the pellet was redispersed in the aqueous medium appropriate for further experimentation.

Fibrin glue. Blood was withdrawn from the mice in a 3.2% w/v sodium tricitrate coated tube to chelate calcium that can lead to instant clotting and centrifuged at 3000 rpm for 2 minutes to extract platelet rich plasma (PRP). Nano/

MicroSera particles were redispersed into 50 µL of a 0.25 M CaCl$_2$ solution in a vial (A). In another vial (B), 25 µL of 5% w/v tranexamic acid and 25 µL of PRP were mixed. The contents of both A and B were mixed and quickly applied over the surgical site.

2.2   Experimentation

The size and surface charge of different nanoparticles were recorded with a Zetasizer instrument (Malvern, U.K.). A transmission electron microscope (JEM 2100) and a field emission scanning electron microscope (JEOL JSM-7610Fplus) were used for imaging and elemental mapping. The fluorescence intensity and cell migration evaluation was done by using ImageJ software. The extinction spectra of PNS in UV-Vis-NIR were recorded from 200 to 1400 nm (Agilent Cary-5000). Proteins extracted from Lap-NanoSera were resolved in 12% polyacrylamide gel and visualized with Coomassie Brilliant Blue staining (Biorad ChemiDoc XRS). The XRD profile of IMQ-MicroSera was recorded using a Bruker ECO D8 Advance diffractometer at room temperature. Bonding confirmation and surface elemental composition of the samples were studied using X-ray photoelectron spectroscopy (K-Alpha plus) in an ultrahigh vacuum chamber (7 × 10^{-9} torr) using Al-Kα radiation (1486.6 Ev).

2.3   Encapsulation efficiency and loading efficiency

The supernatant retrieved during the synthesis process contained the unentrapped drug and was evaluated spectrophotometrically at 319 nm for lapatinib and at 370 nm for imiquimod to calculate encapsulation efficiency (EE%) and loading efficiency (LE%) by an indirect method using the following formula,

$$\text{LE\%} = \frac{\text{initial amount of drug} - \text{amount of drug in the supernatant}}{\text{total weight of nanoparticle}}$$

$$\text{EE\%} = \frac{\text{initial amount of drug} - \text{amount of drug in the supernatant}}{\text{initial amount of drug}}.$$

2.4   Drug release and kinetics

Enzyme-triggered drug release behavior of Lap-NS and IMQ-MS was evaluated by using the sample and separate method.[22] Samples were embedded in Reliseal® along with 1 mL of phosphate buffered saline (PBS) containing proteinase-K (AMBION, Cat. #AM2548) at pH 7.4 (physiological) or pH 6.4 (tumor microenvironment) at 37 °C under constant shaking. At predetermined time points, the supernatant was collected and replaced with the same amount of fresh medium to maintain a constant volume. The withdrawn solution was evaluated spectrophotometrically at 319 nm and 370 nm to obtain the drug concentration released corresponding to Lap-NS and IMQ-MS, respectively.

2.5   SDS-PAGE analysis

Proteins associated with Lap-NS were extracted by incubating with 2× Laemmli buffer (0.125 M tris HCL, 20% glycerol, 4% SDS, 10% β-mercaptoethanol, and 0.004% bromophenol blue). Retrieved proteins were resolved in 12% polyacrylamide gel and visualized (Biorad ChemiDoc XRS) with Coomassie Brilliant Blue staining.

2.6   Photothermal conversion efficiency

The photothermal conversion efficiency was measured for colloidal PNS, PNS in Reliseal® glue and PNS in fibrin glue after irradiation with a 980 nm laser at 660 mW with a distance of 1 cm between the fibre end and the sample vial. Changes in temperature were recorded for 3 cycles with a FLIR ONE Thermal imaging camera. The following formula was used to calculate photothermal conversion efficiency.[23,24]

$$\eta = \frac{hs(T_{\max} - T_{\text{surr}}) - Q_{\text{diss}}}{I(1 - 10^{-A808})}$$

2.7   Cell cytotoxicity assay

The biocompatibility and cytotoxicity of the formulations were tested on L929 fibroblast cells and 4T1 breast cancer cells using MTT (3-(4,5-dimethylthiazol-2-yl)-2,5-diphenyl tetrazolium bromide) assay. Typically, 10^4 cells were incubated in 96 well plates at 37 °C and 5% CO$_2$. At 80% cell density, the culture medium was discarded and replaced with fresh medium containing different concentrations of IMQ-MS (0, 25, 50, 100, 200, and 400 µg mL^{-1}), Lap-NS (0, 0.01, 0.1, 1, 10, and 100 µg mL^{-1}) and PNS (0, 25, 50, 100, 200, and 400 µg mL^{-1}).[20,25,26] Furthermore, 980 nm laser irradiation was administered for 1 min at 0.66 W cm^{-2} in the PNS group. After incubation for 24 h, 48 h and 72 h, the cells were washed and incubated with MTT followed by the solubilization of formazan crystals in DMSO. The absorbance was recorded at 590 nm using the following formula.

$$\text{Cell viability\%} = \frac{\text{absorbance of the treated cells}}{\text{absorbance of the control cells}} \times 100$$

2.8   Apoptosis assay

Cells were treated with imiquimod MicroSera (IMQ-MS) at an IC50 of 206 µg mL^{-1} for 24 h, lapatinib NanoSera (Lap-NS) at an IC50 of 37 µg mL^{-1} for 72 h and PNS + laser at an IC50 of 169 µg mL^{-1} for 24 h. Apoptosis assay as reported by Invitrogen manufacturer catalog no. V13242 was executed by harvesting the cells post-treatments followed by washing with cold PBS, and resuspension in 1× annexin-binding buffer. Furthermore, 5 µL of Alexa Fluor™ 488 annexin V and 1 µL of PI working solution were incubated with 100 µL of cell suspension. Finally, the stained cells were analysed by flow cytometry.

2.9   Monotherapy and combination therapy in a syngeneic 4T1 breast tumor model

All experimentation involving animals was performed after prior approval from the Institutional Animal Ethics Committee (IAEC) at IISER Mohali (Approval no: IISERM/SAFE/PRT/2022/001 and IISERM/SAFE/PRT/2023/006). Throughout the study, the mice were housed in an animal house at IISER Mohali in

individually ventilated cages at a temperature of 22 ± 2 °C and a relative humidity of 50–60% under a 12 h light and dark cycle with access to water and food *ad libitum*. Four week old female BALB/c were subcutaneously injected with 4T1 cells into the mammary fat pad. Once the tumor cells reached around 50 mm^3, they were randomly assigned into the following groups for assessment of tumor regression (n = 5): the immune response group (n = 4–6) and the survival group (n = 5) after the generation of residual tumors. The residual tumor was established by surgically removing ∼95% of the tumor tissue at the surgical site. The contents of Vial A (single or combination of nanoformulations in 50 μL of 0.250 M CaCl$_2$ solution) and B (25 μL of 5% w/v tranexamic acid and 25 μL of PRP) were gently mixed and applied instantly over the surgical site.

Monotherapy groups. Fibrin glue (FG), surgical site application

Saline, intravenous administration

Free dox, intravenous administration, 5 mg kg^{-1}

Free lapatinib, oral administration, 5 mg kg^{-1}

Lap-NS, surgical site application, 5 mg kg^{-1} (ref. 26)

PNS, surgical site application, 20 mg kg^{-1} (ref. 20)

PNSL, surgical site application, 20 mg kg^{-1} + 980 nm laser irradiation for 1 minute

Combination therapy groups. Lap-NS + PNSL, surgical site application

IMQ-MS, surgical site application, 20 mg kg^{-1} (ref. 25)

Nano–MicroSera (Lap-NS (5 mg kg^{-1}) + PNSL (20 mg kg^{-1}) + IMQ-MS (20 mg kg^{-1})) surgical site application

The surgical sites in all groups except those subjected to photothermal therapy were immediately sutured after FG application. Intravenous and oral administrations were performed after stitching of the surgical site without any FG application. For photothermal therapy, after PNS-FG application, the tumor bed was subjected to a 980 nm laser for 1 minute followed by suturing the site. The distance between the tumor bed and the fibre end was 1 cm. The thermal rise was recorded using a FLIR ONE Pro thermal imaging camera. The animals were monitored for body weight and tumor regression for up to 15 days and percentage survival for up to 50 days.

2.10 ICP-MS

Major organs such as the liver, kidneys, heart, lungs, and spleen along with the tumor were excised from the PNS and PNSL groups after day 1 of treatment. All the organs were digested with ICP-MS grade HNO$_3$ at 60° C. The digested samples were then diluted with HPLC grade water and quantified using inductively coupled plasma mass spectrometry.

2.11 Enumerating the percentage of DCs, CD8 T cells and Tregs in the recurred tumor using a flow cytometer

Locally recurred tumors were harvested from the mice on the 5th day post-treatment, followed by the isolation of single-cell suspensions through a 70 μm strainer. The cells were then stained with markers specific to DCs PE anti-mouse CD86 (catalog-105007, Biolegend, San Diego, CA), PE/Cy7 anti-mouse CD11c$^+$ (catalog-117318, Biolegend), and APC anti-mouse

CD80 (catalog-104714, Biolegend)], CD8 T cells [anti-mouse CD8a FITC (11-0081-85)], and Tregs [PE-anti-mouse CD4 and APC anti-mouse FoxP3]. Subsequently, the samples were acquired using BD Accuri (BD Biosciences) and the data were analysed using FlowJo software.

2.12 ELISA

Serum isolated at day 5 post-treatments (groups: 1-FG, 2-Lap + PNSL-FG, 3-IMQ-MS-FG, 4-NMS-FG, and 5-control) was evaluated for IL-6 response with ELISA OptEIA™ mouse IL-6 ELISA assay as per the manufacturer's instruction. Microwells were coated with the capture antibody and incubated overnight at 4 °C followed by washing thrice. The plates were blocked with the assay diluent at RT for 1 h followed by washing 3 times. Standards and samples were added and incubated for 2 h at RT followed by 5 times washing. A wrking detector (detection Ab + Sav-HRP) was added to each well and incubated for 1 h followed by 7 times washing. After that a substrate solution was added and incubated for 30 min at RT in the dark. In the end a stop solution was added to each well and reading was taken at 450 nm within 30 min with a λ correction of 570 nm.

2.13 Histological analysis

An *in vivo* biocompatibility study was conducted at the 50th day for the NMS-FG and control FG groups. The Liver, kidneys, heart, lungs, spleen and tumor were fixed in 10% neutral buffer formalin. 5 μm thin sections were trimmed and stained with haematoxylin and eosin dye. The sections were examined under an Olympus light microscope.

2.14 Statistical analysis

All the data values were recorded and represented as mean ± standard deviation. One-way ANOVA was performed for calculating statistical significance.

3. Results and discussion

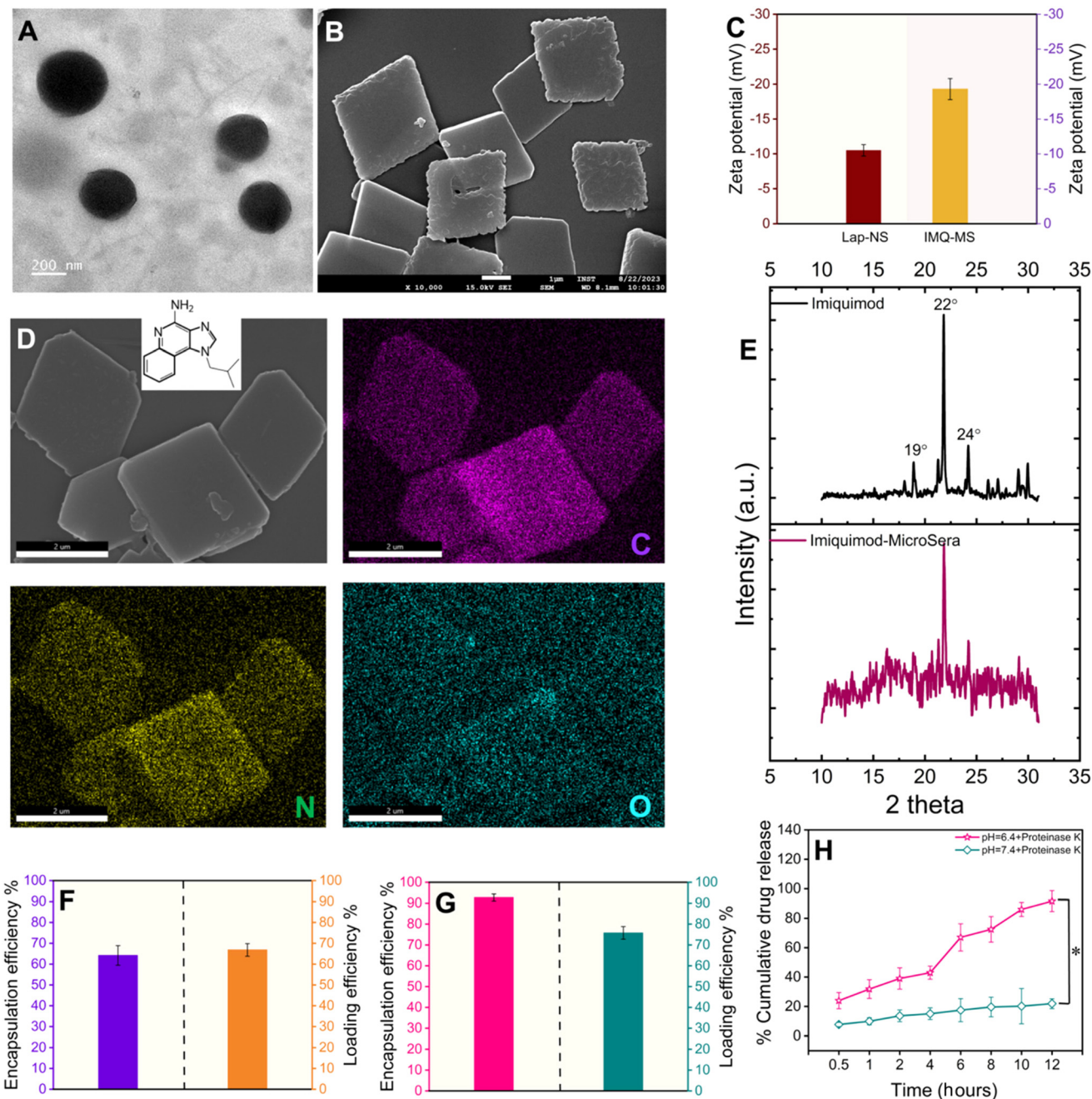### 3.1 Synthesis and characterization of Lap-NS, PNS and IMQ-MS

A liquid antisolvent (LAS) precipitation technique was utilized for dispersing hydrophobic and low permeability class IV drugs, lapatinib (Lap) and imiquimod (IMQ), in aqueous medium. A homogeneous solution of serum proteins in aqueous medium was exposed to the antisolvent DMSO, which had either Lap or IMQ dissolved in it. This led to nucleation and coagulation or condensation of the drug.[27,28] Further growth and agglomeration of the drug were halted with rapid centrifugation of the mixture yielding nano- and microcrystals of lapatinib (lapatinib-NanoSera or Lap-NS) and imiquimod (imiquimod-MicroSera or IMQ-MS), respectively. In aqueous medium, serum proteins function as stabilizers and provide surface coverage to enhance the hydrophilicity of the drug formulation. The synthesis process excludes additional surfactants or cross-linkers, involving only minimal components such as the drug and whole serum proteins.[19] Through a straightforward LAS process, which entails mixing serum and

DMSO containing lapatinib under optimal conditions, spherical Lap-NS with a diameter of approximately 250 nm and a surface charge of around −10 mV were successfully formed (Fig. 2A, S1† and 2C). XPS analysis revealed elemental composition corresponding to both Lap and serum proteins (Fig. S1†).

On the other hand, LAS assisted with high-speed probe homogenization induced IMQ to aggregate into a rhombic microplate morphology possessing an average diagonal length of ∼3.6 × 3.4 μm and a thickness of ∼0.2 μm with a surface charge of ∼−19 mV (Fig. 2B and C). Elemental mapping confirmed a trace of oxygen, the third most abundant element present in proteins, on the IMQ-MS (Fig. 2D). The negative surface charge is expected to be imparted with the adsorption of serum proteins on IMQ-MS. Furthermore, XRD analysis revealed that IMQ-MS had characteristic 2θ peaks at 19°, 22° and 24° of unprocessed imiquimod crystals. This confirms the

Fig. 2 Characterization of lapatinib-NanoSera (Lap-NS) and imiquimod-MicroSera (IMQ-MS). (A) TEM image of LAP-NS; (B) FESEM image of IMQ-MS; (C) surface charge of Lap-NS and IMQ-MS; (D) elemental mapping of IMQ-MS; (E) X-ray diffraction patterns of IMQ and IMQ-MS; encapsulation and loading efficiency of (F) Lap-NS and (G) IMQ-MS; and (H) lapatinib release kinetics in the presence of proteinase K at pH 7.4 and 6.4 from Lap-NS.

retention of its crystalline nature even after downsizing to a specific morphology (Fig. 2E).[29] Similarly, Lap-NS also revealed a typical 2θ peak at 23°, demonstrating a crystalline order (Fig. S2†).[30] This crystallization of hydrophobic drugs as nano- or micro-particles is known to achieve high loading (50–90%) compared to physical entrapment in a carrier matrix.[31] The Lap-NS was quantified to possess an encapsulation and loading efficiency of ~67% and ~64% respectively (Fig. 2F). Similarly, IMQ-MS also showed a distinctly high encapsulation efficiency of ~93% and a loading content of ~76%, which is higher than the previously reported drug loading for imiquimod formulation (Fig. 1G).[32]

Additionally, we employed a platelet-rich plasma (PRP)-based fibrin glue as the reservoir for the localized release of the drug from Lap-NS or/and IMQ-MS within the tumor bed. To achieve this, pooled PRP obtained from BALB/c mice was combined with tranexamic acid (TXA) to counteract instant fibrinolysis within a vial. Following this, Lap-NS or/and IMQ-MS in calcium chloride solution was prepared and then blended with the PRP-TXA solution to facilitate the formation of the fibrin glue (Fig. S3A†). Calcium helps in the quick activation of the coagulation cascade within the PRP and aids in the formation of the hybrid fibrin glue.[33] Fig. S3B† shows a highly porous fibrin network as analyzed using FESEM. Next, the release kinetics of the loaded drug from the hybrid fibrin glue was studied under the physiological (pH 7.4) and tumor microenvironment (pH 6.4) conditions. As fibrin glue will be applied topically on the tumor bed, plasmin present in excess post-surgery causes proteolytic degradation of the fibrin clots to release the drug.[34] To simulate such conditions, proteinase-K was added to the release reservoir. As seen in Fig. 2H, a cumulative accelerated release of lapatinib up to ~89% at pH 6.4 and a slow release of ~19% at pH 7.4 were observed within 12 h. Imiquimod followed a similar pattern with a cumulative release of ~92% at pH 6.4 and ~23% at pH 7.4 (Fig. S4†). While proteolytic cleavage might loosen up the fibrin clot, pH played a major role in dissolving the nano- and micro-particles.

Lap-NS prepared with serum from three distinct healthy human donors were assessed for protein abundance and composition. SDS-PAGE analysis revealed a differential association of proteins from distinctive donors (Fig. S5†). In concurrence with our previous report, the major protein fingerprint associated with Lap-HS was albumin, globulin and apolipoprotein with variable contents. While albumin is a known drug carrier, apolipoproteins provide a stealth effect counterbalancing the opsonization effect of the globulins.[19,20,35,36]

We further incorporated gold nanodendrites termed plasmonic nanosera (PNS) into the fibrin glue after preparing them as per the method reported by our group.[20] The evolution of PNS from first generation branches to a densely branched anisotropic nanodendritic morphology was confirmed using TEM (Fig. 3A and B). PNS synthesized with serum from different sources such as human, mouse and bovine was found to give a broad absorption in visible to near infrared (I & II) windows (Fig. S6†). HRTEM analysis verified the *d*-spacing of the predominant {111} lattice plane and

selected-area electron diffraction (SAED) pattern representing the face-centered cubic structure of gold in the PNS (Fig. S7†).[37] Elemental mapping of PNS confirmed the commingled existence of serum proteins with the presence of both nitrogen and oxygen (Fig. 3C). The photothermal transduction of PNS was studied in both colloidal and fibrin entrapped forms by irradiating with a 980 nm laser at 0.660 W. The colloidal PNS caused a temperature rise of ~81 °C after five minutes of irradiation with a ~67% photothermal conversion efficiency (Fig. 3D and E). For fibrin entrapment, the commercial fibrin glue Reliseal® and human derived PRP fibrin glue were compared. PNS in the Reliseal® caused a temperature rise of ~51 °C in five minutes.
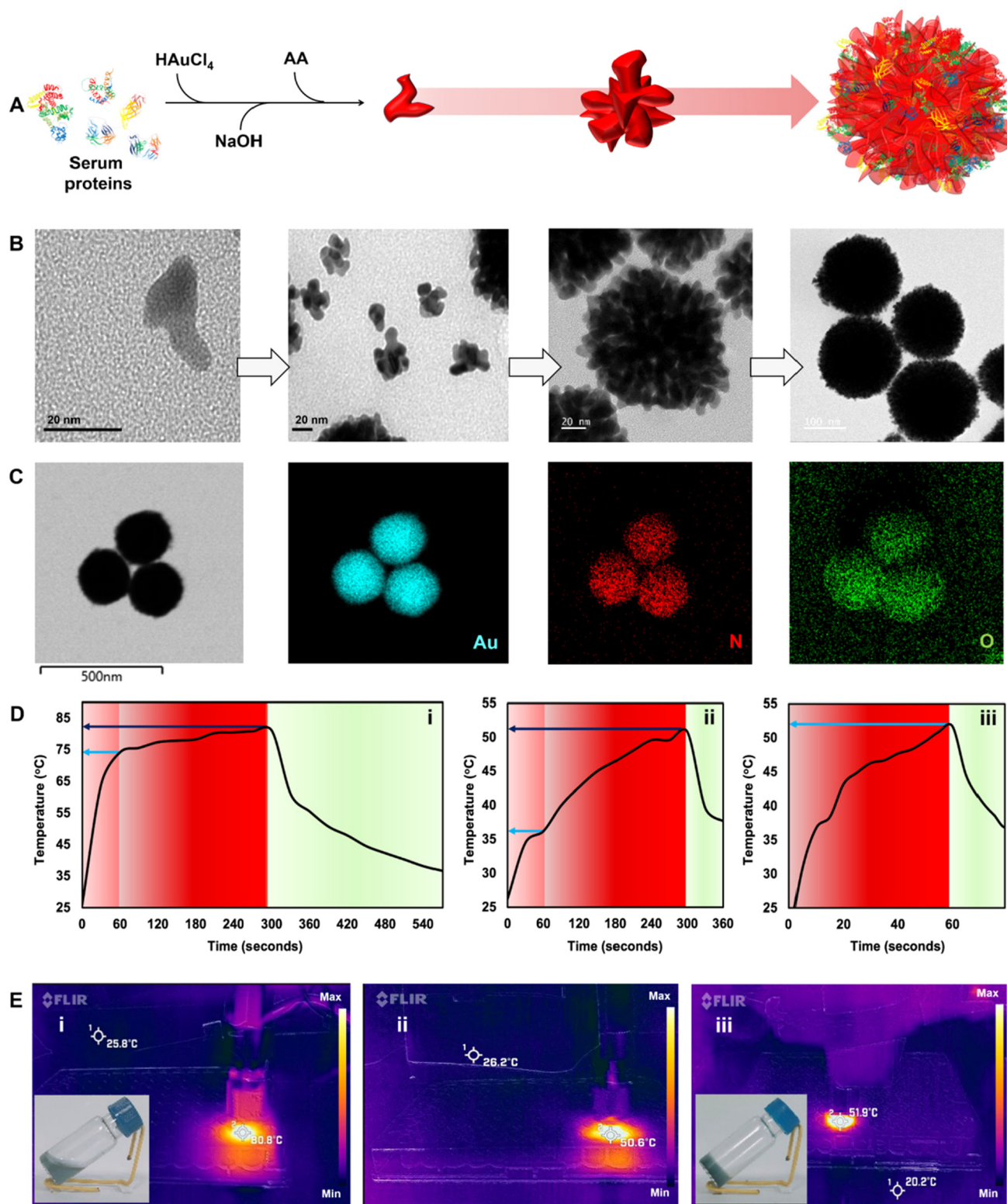
The decrease in the achieved temperature could be due to the low thermal conductivity of fibrin compared to that of water.[38] While the PRP fibrin glue embedded PNS demonstrated a comparable temperature rise within one minute of irradiation, it is worth noting that the scattering from platelets may contribute to this rapid increase in temperature. However, it is important to consider that blood and tissue components typically exhibit thermal conductivity lower than that of water.[39] Thus the rise in temperature observed from the PRP fibrin glue is still ~22 °C lower than that of the colloidal PNS (~74 °C) at one minute. Nevertheless, the photothermal transduction achieved by the PRP fibrin glue in this short duration is enough to cause irreversible vascular thrombosis, ischemia, and hypoxia leading to cancer cell death.[40]

3.2 Induction of cancer cell apoptosis with NanoSera and MicroSera

The formulations were evaluated for their anticancer effect on 4T1 breast cancer cells. A dose dependent reduction in the 4T1 cell viability (Fig. 4A, B and C) was observed with an IC50 of 206 μg mL^{-1} for IMQ-MS at 24 h and 37 μg mL^{-1} for Lap-NS at 72 h and 169 μg mL^{-1} for PNS + laser at 24 h. After treatment with their respective IC50 concentrations, the cells showed significant population in early apoptosis with no signs of necrosis, signifying a systematic programmed cell death induction (Fig. 4D).
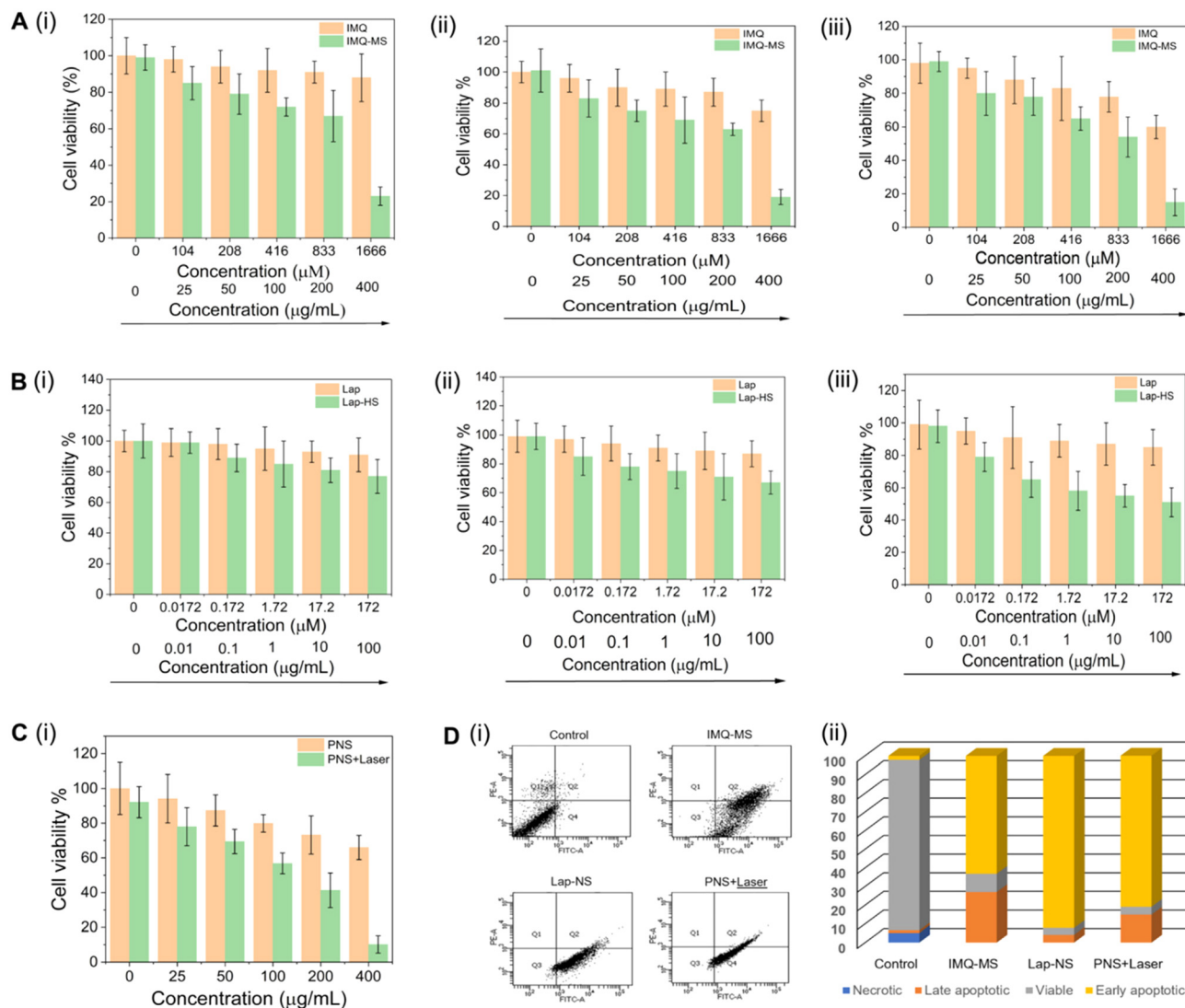
3.3 Lapatinib or plasmonic NanoSera based localized monotherapy

The mice were subjected to breast conservation surgical removal of up to ~95% 4T1 tumor followed by treatment with blank fibrin glue, hybrid fibrin glue, and saline in the tumor bed before suturing the surgical site (Fig. 5B and ESI Video 1†). Clinically relevant adjuvant chemotherapy controls were also concurrently evaluated after tumor resection with doxorubicin (i.v) and lapatinib (p.o). Preliminary evaluation of the biodistribution of Lap-NS and PNS in vital organs (spleen, tumor, liver, heart and kidneys) was performed following their localized implantation. One day post-implantation, systemic spillage of ICG doped Lap-NS was traced to different organs. *Ex vivo* fluorescence imaging revealed that in comparison with the rapid clearance of physically entrapped free ICG from autologous fibrin glue, Lap-NS showed delayed ICG release as con-

Fig. 3 Characterization of plasmonic NanoSera (PNS). (A) Schematic of PNS formation; (B) different stages of PNS growth; (C) elemental mapping of PNS; (D) heating (red)–cooling (green) plots and (E) corresponding thermal images of PNS (i) in water, (ii) in Reliseal® and (iii) in PRP fibrin glue under 980 nm irradiation (dark blue and white arrows indicate the temperature at 300 and 60 seconds, respectively). Inset images show PNS (i) in water and (iii) in PRP fibrin glue.
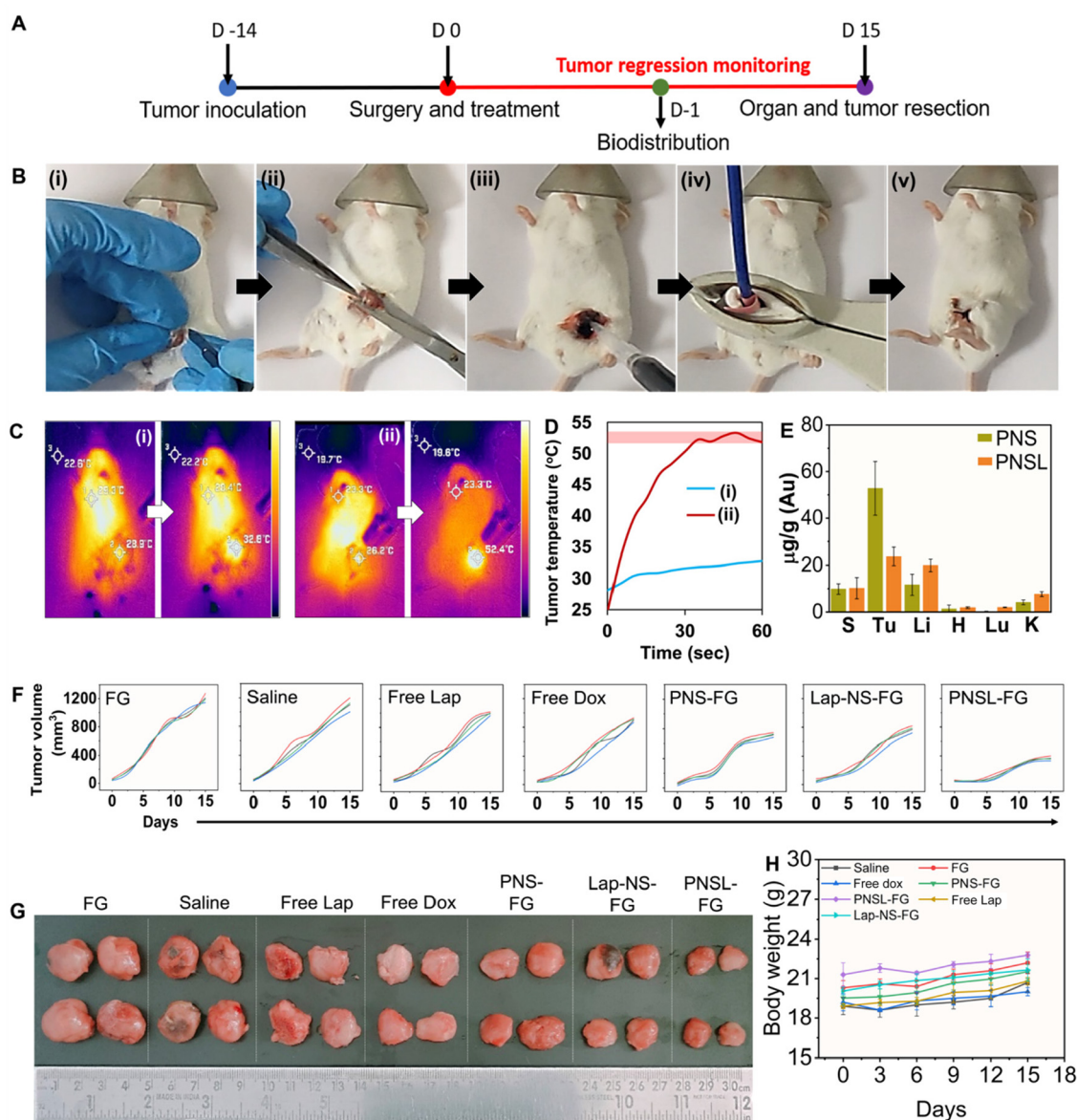
Fig. 4 *In vitro* anticancer efficacy of IMQ-MS (A), Lap-NS (B) and PNS (C) at (i) 24 h (ii) 48 h and (iii) 72 h; (D) annexin V-FITC/PI staining analysis with flow cytometry shows different cell populations (Q1-necrotic cells, Q2-late apoptotic cells, Q3-viable cells and early apoptotic cells) after treatment with the NanoSera and MicroSera.

firmed by the fluorescence chiefly in the liver and spleen (Fig. S9†). As established from the *in vitro* release kinetics of Lap, an elevated level of proteases in the tumor bed can degrade the NanoSera into smaller sizes and/or a free form of the drug to be redistributed *via* angiogenic blood vessels into different organs.[41] Its presence in the liver and kidneys is suggestive of predominant hepatobiliary and secondary renal elimination of lapatinib.[42] However, the reticuloendothelial system (RES) mediated clearance can potentially deliver any non-degraded Lap-NS to the liver and spleen.

Laser irradiation (980 nm) immediately after the implantation of PNS laced fibrin glue for one minute resulted in the localized temperature rise of ~52 °C as compared to ~4 °C in blank fibrin glue (Fig. 5C and D). Quantitative analysis of gold in various organs using ICP-MS indicated more clearance of PNS after laser irradiation in comparison with that in the

absence of irradiation (Fig. 5E). Hyperthermia causes vascular perfusion resulting in enhanced systemic leakage and distribution of PNS chiefly in the liver and spleen followed by the kidneys after 24 h of implantation.[43] Despite the rapid clearance of NanoSera particles, their acute availability in the implantation site imparted a significant effect on the residual tumor cells impeding their local regrowth. Compared to conventional therapy such as intravenous administration of doxorubicin and oral intake of lapatinib, localized chemotherapy with Lap-NS or photothermal therapy with PNS of the tumor bed showed considerable tumor inhibition. Particularly, photothermal therapy showed consequential suppression due to thermal ablation of tumor cells (Fig. 5F and G). Thermal ablation induced by PNS alters the architecture of the tumor microenvironment, potentially enhancing the penetration of chemotherapeutic and immunomodulatory agents.[44]
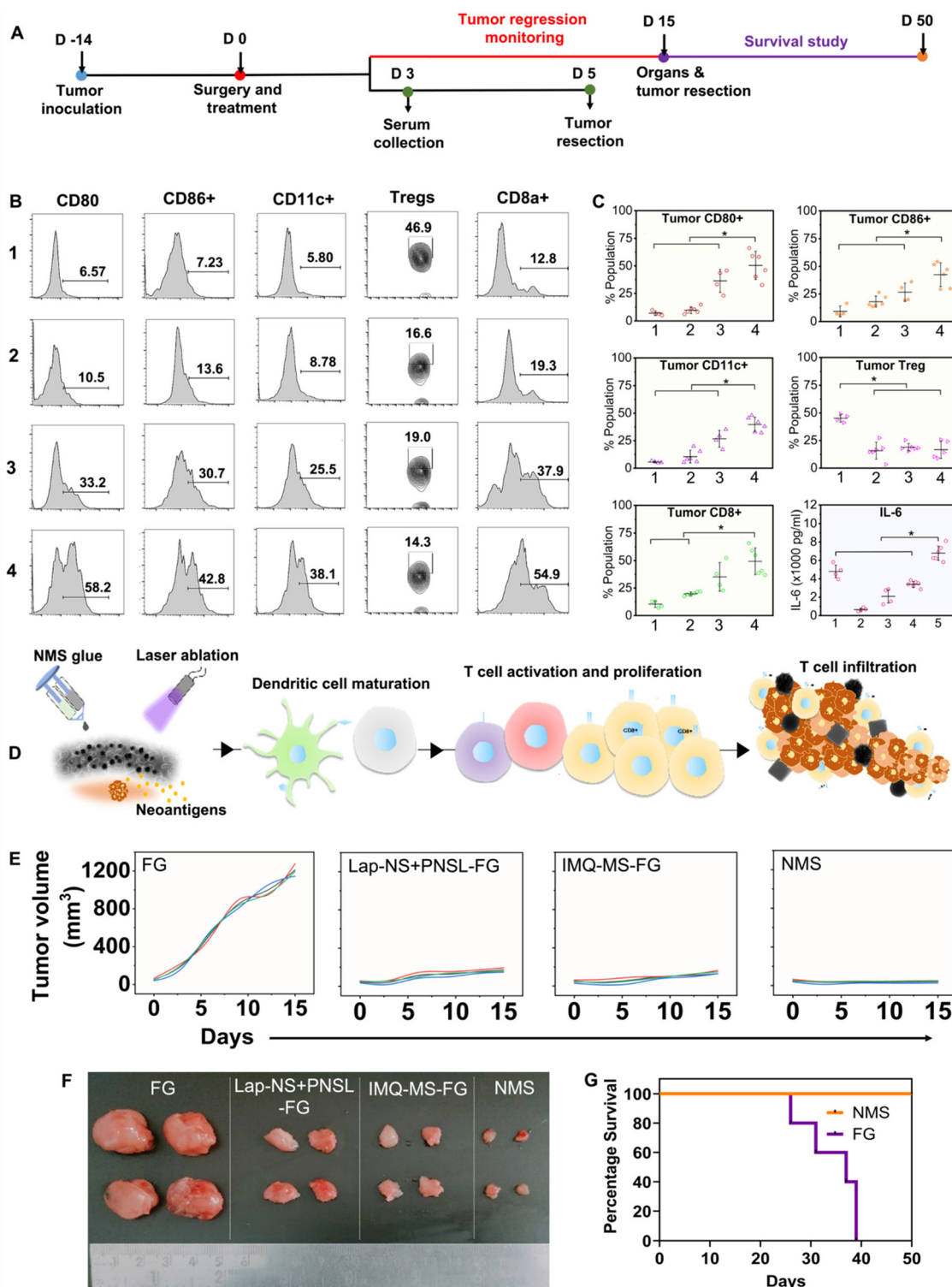
Fig. 5 Tumor regression analysis with monotherapy. (A) Timeline of residual tumor generation and local tumor regression after different treatments; (B) surgical procedure showing (i) incision, (ii) 4T1 tumor resection, (iii) hybrid glue application, (iv) laser irradiation and (v) closure of the surgical site; (C) thermal imaging and (D) tumor temperature after application and laser irradiation of (i) blank fibrin glue (FG) and (ii) PNS-FG; (E) biodistribution of PNS (without laser irradiation) and PNSL (with laser irradiation) in various organs after 24 h post-application at the surgical site; (F) change in tumor volume in different groups; (G) images of the locally recurred tumor excised from mice in the different groups; and (H) body weight of mice in different groups over the study duration (*$p \leq 0.05$).

Furthermore, thermotherapy initiates the softening of tumors, reverses tumor rigidification, and ablates physical barriers, thereby improving the efficacy of drugs for therapeutically resistant tumors.[45] Throughout the treatment period, the mice exhibited normal overall health, as indicated by stable body weight measurements (Fig. 5H).

3.4 Nano–MicroSera based localized combination of chemo-photothermal immune stimulation

Although thermal shock may effectively control tumor recurrence, one must consider that cancer cells situated deeply

from the surface of the implantation may evade the effects due to thermal insulation from surrounding cells, potentially leading to local recurrence in the long term. However, cancer cells directly impacted by chemotherapy and photothermal therapy undergo immunogenic cell death (ICD), releasing tumor antigens. These antigens have the potential to stimulate dendritic cell (DC) maturation and subsequently trigger T cell activation and differentiation, resulting in targeted elimination of residual deep-seated cancer cells.[46] However, the tumor microenvironment is immunosuppressive, primarily because of the presence and coordination of a tightly regulated system

Fig. 6 Tumor regression analysis with combination therapy. (A) timeline of Nano−MicroSera based localized chemo-photothermal immune stimulation and local tumor regression analysis. (B) & (C) Percentage population of dendritic cells (CD80+, CD86+, and CD11c+), regulatory T-cells (CD4+ FoxP3+) and cytotoxic T-cells (CD8a+) in recurrent tumors collected at day 5 and serum IL-6 levels at day 3 post-treatment (1-FG, 2-Lap + PNSL-FG, 3-IMQ-MS-FG, 4-NMS-FG, and 5-Control) (n = 4 to 6); (D) illustration of localized immune response with NMS-FG; (E) change in tumor volume in the different groups; (F) images of locally recurred tumor excised from mice in the different groups; and (G) percentage survival of mice treated with blank FG and NMS-FG (n = 5), *$p \leq 0.05$.

involving T regulatory cells (Tregs), tumor-associated macrophages, and cytokines such as TGF-β and IL-10. This environment accelerates tumor growth and facilitates evasion of the immune response.[47,48] Incorporating immune adjuvants such as IMQ into the treatment regimen can help overcome this immunosuppressive barrier and enhance the potency of tumor antigen-mediated anti-tumor immune responses.

While IMQ is utilized as an immune response modifier, it also has the capacity to directly trigger apoptosis in cancer cells as demonstrated in the *in vitro* experiments. This cell death mechanism associated with IMQ is linked to the upregulation of pro-apoptotic proteins within the Bcl-2 family, including BH3-only proteins.[49,50] The antigens released from apoptotic cell death can additionally enhance the anti-tumor activity of IMQ through TLR7/8-mediated activation of DCs. This activation leads to the recruitment of cytotoxic CD8^{+} T cells and killing of tumor cells. The implantation of IMQ-MS-based autologous fibrin glue, in conjunction with surgery-induced tumor antigens, prompted the maturation and expansion of the pool of CD11c^{+} DCs (Fig. 6B, C and Fig. S10†). This was evidenced by the upregulation of co-stimulatory molecules such as CD80^{+} and CD86^{+} (Fig. 6B, C and Fig. S11, 12†). Furthermore, the serum levels of cytokine IL-6 and TNF-α were noticed to be significantly altered in the treatment groups (Fig. 6C and Fig. S13†). The modulation observed in the immune system suggests the involvement of parameters crucial for protecting against tumors.[51] The results noted five days after implantation were consistent, regardless of the acute availability of IMQ-MS at the tumor bed. However, it is worth noting that IMQ-MS exhibited rapid clearance to the lungs, which is attributed to the tendency of micron-sized particles to passively accumulate in this organ (Fig. S9†).[52–54]

Another important observation noted was the significant decline in the percent of Tregs (Fig. 6B, C and Fig. S14†). Tregs are indeed known to facilitate the progression of cancer cells. However, the combination of chemo-photothermal immune stimulation with Nano–MicroSera (NMS: Lap-NS + PNS + IMQ-MS) based hybrid fibrin glue led to enhanced maturation of DCs and suppression of Tregs (Fig. 6C). As a result, the tumor size was markedly reduced in the NMS-treated mice. This significant reduction in tumor size was closely correlated with an increase in the number of CD8 T cells and a decrease in Tregs (Fig. 6E, F and Fig. S15†). The combination immunotherapy group demonstrated an exceptional immune response, which is attributed to both the superior cancer cell-killing effect of chemo-photothermal therapy (Fig. 6D). Remarkably, the body weight of mice in the treatment groups remained unaffected (Fig. S16†). Subsequently, the NMS based hybrid fibrin glue implanted mice were found to show 100% survival, after 50 days of treatment. Histological analysis of the surviving mice revealed unaltered microstructures of their major organs (Fig. S17†).

This study suggests that a therapeutic hybrid fibrin glue offers a promising solution for addressing local recurrence in early-stage triple-negative breast cancer. Combining high drug-loaded lapatinib-NanoSera and imiquimod-MicroSera with plasmonic NanoSera, we achieved superior tumor inhibition and enhanced survival outcomes through localized combination immunotherapy. Furthermore, the activation of DCs and CD8 T cells implies the potential elimination of hidden and residual tumor cells. This strategy holds promise for paving the way toward successful cancer treatment in the future.

4. Conclusion

Our all-in-one autologous approach represents a novel strategy involving the modification of therapeutic nano/micromaterials with patient or donor derived serum proteins as stabilizers, tailored for localized intra-operative application in the surgical tumor bed to facilitate post-surgical management. The autologous hybrid fibrin glue exhibited remarkable synergy and superior outcomes in suppressing recurrent breast tumors. This host-specific approach is meticulously crafted for bedside fabrication using minimal resources, addressing the limitations of conventional therapies and ensuring accessibility for patients across the economic hierarchy. Further improvement in the therapeutic activity is possible by enhancing the cargo residence time by reinforcing the fibrin structures with stabilizers that bind to the amide backbone for delayed proteolytic degradation. The highly porous nature of the PNS might enable their biological degradation as demonstrated earlier in smaller gold nanoparticles,[55] possibly within the biodistributed highly metabolic organs such as the liver. However, any recrystallization of the released gold chelates of metallothionine and glutathione implies long term persistence and requires careful evaluation. Finally, dose escalated efficacy and safety studies in large animal models would further validate the clinical translation of this potential approach.

Ethics statement

Data availability

All raw data will be made available by the authors on reasonable request.

Author contributions

Mimansa performed the synthesis and characterization of the nanoparticles followed by carrying out the *in vitro* and *in vivo*

experiments; curated the data; performed formal analysis and drafted the manuscript. Mohammad Adeel Zafar contributed to the assessment and analysis of immune stimulatory markers in animals. Dr Reena Das and Dr Dinesh K Verma provided conceptual and physical resources for the study. Dr Javed N Agrewala coordinated the immunological assessments and edited the manuscript. Dr Asifkhan Shanavas conceptualized and coordinated the project, managed resources, and reviewed and edited the manuscript. All authors approved the final manuscript.

Conflicts of interest

The authors declare no conflict of interest.

Acknowledgements

References

1 M. Riis, Modern Surgical Treatment of Breast Cancer, *Ann. Med. Surg.*, 2020, **56**, 95–107, DOI: **10.1016/j.amsu.2020.06.016**.

2 S. Keelan, M. Flanagan and A. D. K. Hill, Evolving Trends in Surgical Management of Breast Cancer: An Analysis of 30 Years of Practice Changing Papers, *Front. Oncol.*, 2021, **11**, 622621, DOI: **10.3389/fonc.2021.622621**.

3 N. M. Almansour, Triple-Negative Breast Cancer: A Brief Review About Epidemiology, Risk Factors, Signaling Pathways, Treatment and Role of Artificial Intelligence, *Front. Mol. Biosci.*, 2022, **9**, 836417, DOI: **10.3389/fmolb.2022.836417**.

4 P. Zagami and L. A. Carey, Triple Negative Breast Cancer: Pitfalls and Progress, *npj Breast Cancer*, 2022, **8**(1), 95, DOI: **10.1038/s41523-022-00468-0**.

5 A. R. T. Bergin and S. Loi, Triple-Negative Breast Cancer: Recent Treatment Advances, *F1000Research*, 2019, **8**, 1342, DOI: **10.12688/f1000research.18888.1**.

6 C. M. Siamof, S. Goel and W. Cai, Moving Beyond the Pillars of Cancer Treatment: Perspectives From Nanotechnology, *Front. Chem.*, 2020, **8**, 598100, DOI: **10.3389/fchem.2020.598100**.

7 T. Iuchi, A. Inoue, Y. Hirose, M. Morioka, K. Horiguchi, A. Natsume, Y. Arakawa, K. Iwasaki, M. Fujiki, T. Kumabe and Y. Sakata, Long-Term Effectiveness of Gliadel Implant for Malignant Glioma and Prognostic Factors for Survival: 3-Year Results of a Postmarketing Surveillance in Japan, *Neuro Oncol Adv.*, 2022, **4**(1), 1–11, DOI: **10.1093/noajnl/vdab189**.

8 N. L. Elstad and K. D. Fowers, OncoGel (ReGel/Paclitaxel)—Clinical Applications for a Novel Paclitaxel Delivery System, *Adv. Drug Delivery Rev.*, 2009, **61**(10), 785–794, DOI: **10.1016/j.addr.2009.04.010**.

9 H. Yuan, B. Zheng and S. Tu, Clinical Research of Intraperitoneal Implantation of Sustained-Release 5-Fluorouracil in Advanced Colorectal Cancer, *World J. Surg. Oncol.*, 2015, **13**, 320, DOI: **10.1186/s12957-015-0737-9**.

10 A. A. Exner and G. M. Saidel, Drug-Eluting Polymer Implants in Cancer Therapy, *Expert Opin. Drug Delivery*, 2008, **5**(7), 775–788, DOI: **10.1517/17425247.5.7.775**.

11 A. R. Johnson, S. P. Forster, D. White, G. Terife, M. Lowinger, R. S. Teller and S. E. Barrett, Drug Eluting Implants in Pharmaceutical Development and Clinical Practice, *Expert Opin. Drug Delivery*, 2021, **18**(5), 577–593, DOI: **10.1080/17425247.2021.1856072**.

12 M. Beudert, M. Gutmann, T. Lühmann and L. Meinel, Fibrin Sealants: Challenges and Solutions, *ACS Biomater. Sci. Eng.*, 2022, **8**(6), 2220–2231, DOI: **10.1021/acsbiomaterials.1c01437**.

13 S. Wilhelm, A. J. Tavares, Q. Dai, S. Ohta, J. Audet, H. F. Dvorak and W. C. W. Chan, Analysis of Nanoparticle Delivery to Tumours, *Nat. Rev. Mater.*, 2016, **1**(5), 16014, DOI: **10.1038/natrevmats.2016.14**.

14 Q. Chen, C. Wang, X. Zhang, G. Chen, Q. Hu, H. Li, J. Wang, D. Wen, Y. Zhang, Y. Lu, G. Yang, C. Jiang, J. Wang, G. Dotti and Z. Gu, In Situ Sprayed Bioresponsive Immunotherapeutic Gel for Post-Surgical Cancer Treatment, *Nat. Nanotechnol.*, 2019, **14**(1), 89–97, DOI: **10.1038/s41565-018-0319-4**.

15 M. J. Tappin, S. Sánchez-Tabernero and F. Sabatino, Glue and Glide: A Novel Technique for Pterygium Conjunctival Autograft, *Clin. Ophthalmol.*, 2018, **13**, 25–26, DOI: **10.2147/OPTH.S191833**.

16 N. Bhavsar, B. Jathal and A. Trivedi, Use of Fibrin Glue in Periodontal Flap Surgery, *J. Indian Soc. Periodontol.*, 2008, **12**(1), 21, DOI: **10.4103/0972-124X.44094**.

17 K. K. Middleton, V. Barro, B. Muller, S. Terada and F. H. Fu, Evaluation of the Effects of Platelet-Rich Plasma (PRP) Therapy Involved in the Healing of Sports-Related Soft Tissue Injuries, *Iowa Orthop. J.*, 2012, **32**, 150–163.

18 T. Domenech and P. S. Doyle, High Loading Capacity Nanoencapsulation and Release of Hydrophobic Drug Nanocrystals from Microgel Particles, *Chem. Mater.*, 2020, **32**(1), 498–509, DOI: **10.1021/acs.chemmater.9b04241**.

19 Mimansa, M. Jamwal, R. Das and A. Shanavas, High Drug Loading Nanoparticles Stabilized with Autologous Serum Proteins Passively Inhibits Tumor Growth, *Biomacromolecules*, 2022, **23**(12), 5065–5073, DOI: **10.1021/acs.biomac.2c00907**.

20 Mimansa, S. Bansal, P. Yadav and A. Shanavas, Plasmonic Nanodendrites Stabilized with Autologous Serum Proteins for Sustainable Host Specific Photothermal Tumor Ablation, *Mater. Adv.*, 2023, **4**, 6175, DOI: 10.1039/D3MA00576C.

21 K. Sood, P. Yadav, M. Jamwal, R. Das and A. Shanavas, Preclinical Safety Assessment of Photoluminescent Metal Quantum Clusters Stabilized with Autologous Serum Proteins for Host Specific Theranostics, *Nanotheranostics*, 2023, **7**(3), 316–326, DOI: 10.7150/ntno.82978.

22 J. Shen and D. J. Burgess, In Vitro Dissolution Testing Strategies for Nanoparticulate Drug Delivery Systems: Recent Developments and Challenges, *Drug Delivery Transl. Res.*, 2013, **3**(5), 409–415, DOI: 10.1007/s13346-013-0129-z.

23 Q. Tian, F. Jiang, R. Zou, Q. Liu, Z. Chen, M. Zhu, S. Yang, J. Wang, J. Wang and J. Hu, Hydrophilic Cu_9S_5 Nanocrystals: A Photothermal Agent with a 25.7% Heat Conversion Efficiency for Photothermal Ablation of Cancer Cells *in Vivo*, *ACS Nano*, 2011, **5**(12), 9761–9771, DOI: 10.1021/nn203293t.

24 X. Liu, B. Li, F. Fu, K. Xu, R. Zou, Q. Wang, B. Zhang, Z. Chen and J. Hu, Facile Synthesis of Biocompatible Cysteine-Coated CuS Nanoparticles with High Photothermal Conversion Efficiency for Cancer Therapy, *Dalton Trans.*, 2014, **43**(30), 11709, DOI: 10.1039/C4DT00424H.

25 R. Chang, X. Chu, J. Zhang, R. Fu, C. Feng, D. Jia, R. Wang, H. Yan, G. Li and J. Li, Liposome-Based Co-Immunotherapy with TLR Agonist and CD47-SIRPα Checkpoint Blockade for Efficient Treatment of Colon Cancer, *Molecules*, 2023, **28**(7), 3147, DOI: 10.3390/molecules28073147.

26 H. Lu, T. Chen, Y. Wang, Y. He, Z. Pang and Y. Wang, Dual Targeting Micelles Loaded with Paclitaxel and Lapatinib for Combinational Therapy of Brain Metastases from Breast Cancer, *Sci. Rep.*, 2022, **12**(1), 2610, DOI: 10.1038/s41598-022-06677-8.

27 A. A. Thorat and S. V. Dalvi, Liquid Antisolvent Precipitation and Stabilization of Nanoparticles of Poorly Water Soluble Drugs in Aqueous Suspensions: Recent Developments and Future Perspective, *Chem. Eng. J.*, 2012, **181–182**, 1–34, DOI: 10.1016/j.cej.2011.12.044.

28 M. E. Matteucci, M. A. Hotze, K. P. Johnston and R. O. Williams, Drug Nanoparticles by Antisolvent Precipitation: Mixing Energy versus Surfactant Stabilization, *Langmuir*, 2006, **22**(21), 8951–8959, DOI: 10.1021/la061122t.

29 P. D. F. R. Remiro, P. D. T. V. E. Rosa and Â.M Moraes, Effect of Process Variables on Imiquimod Micronization Using a Supercritical Antisolvent (SAS) Precipitation Technique, *J. Supercrit. Fluids*, 2022, **181**, 105500, DOI: 10.1016/j.supflu.2021.105500.

30 P. P. Prabhu, Prathvi, T. V. Gujaran, C. H. Mehta, A. Suresh, K. B. Koteshwara, K. G. Pai and U. Y. Nayak, Development of Lapatinib Nanosponges for Enhancing Bioavailability, *J. Drug Delivery Sci. Technol.*, 2021, **65**, 102684, DOI: 10.1016/j.jddst.2021.102684.

31 Z. Chen, W. Wu and Y. Lu, What Is the Future for Nanocrystal-Based Drug-Delivery Systems?, *Ther. Delivery*, 2020, **11**(4), 225–229, DOI: 10.4155/tde-2020-0016.

32 A. Almomen, M. Badran, A. A. Alhowyan, M. Alkholief and A. Alshamsan, Imiquimod-Loaded Chitosan-Decorated Di-Block and Tri-Block Polymeric Nanoparticles Loaded In Situ Gel for the Management of Cervical Cancer, *Gels*, 2023, **9**(9), 713, DOI: 10.3390/gels9090713.

33 T. Toyoda, K. Isobe, T. Tsujino, Y. Koyata, F. Ohyagi, T. Watanabe, M. Nakamura, Y. Kitamura, H. Okudera, K. Nakata and T. Kawase, Direct Activation of Platelets by Addition of $CaCl_2$ Leads Coagulation of Platelet-Rich Plasma, *Int. J. Implant Dent.*, 2018, **4**(1), 23, DOI: 10.1186/s40729-018-0134-6.

34 J. W. Weisel and R. I. Litvinov, Fibrin Formation, Structure and Properties, in *Fibrous Proteins: Structures and Mechanisms*, ed. D. A. D. Parry and J. M. Squire, Springer International Publishing, Cham, 2017, vol. 82, pp. 405–456. Subcellular Biochemistry. DOI: 10.1007/978-3-319-49674-0_13.

35 P. Lee and X. Wu, Review: Modifications of Human Serum Albumin and Their Binding Effect, *Curr. Pharm. Des.*, 2015, **21**(14), 1862–1865.

36 S. Schöttler, G. Becker, S. Winzen, T. Steinbach, K. Mohr, K. Landfester, V. Mailänder and F. R. Wurm, Protein Adsorption Is Required for Stealth Effect of Poly(Ethylene Glycol)- and Poly(Phosphoester)-Coated Nanocarriers, *Nat. Nanotechnol.*, 2016, **11**(4), 372–377, DOI: 10.1038/nnano.2015.330.

37 G. Liu, S. Wang, S. Wang, R. Wu, H. Li, M. Zha, J. Song, Y. Yin, K. Li, J. Mu and Y. Shi, Carbon Dots-Mediated Synthesis of Gold Nanodendrites with Extended Absorption into NIR-II Window for in Vivo Photothermal Therapy, *J. Nanobiotechnol.*, 2023, **21**(1), 151, DOI: 10.1186/s12951-023-01887-2.

38 A. Mollahosseini and A. Abdelrasoul, Assessment of Fibrinogen Thermal Conductivity and Interaction Energy with Polyarylethersulfone (PAES) Clinical Hemodialysis Membranes at Normal and Elevated Patient Body Temperatures, *C*, 2023, **9**(1), 33, DOI: 10.3390/c9010033.

39 E. Ponder, The Coefficient of Thermal Conductivity of Blood and of Various Tissues, *J. Gen. Physiol.*, 1962, **45**(3), 545–551, DOI: 10.1085/jgp.45.3.545.

40 C. Brace, Thermal Tumor Ablation in Clinical Use, *IEEE Pulse*, 2011, **2**(5), 28–38, DOI: 10.1109/MPUL.2011.942603.

41 Y. Itoh, Proteolytic Modulation of Tumor Microenvironment Signals during Cancer Progression, *Front. Oncol.*, 2022, **12**, 935231, DOI: 10.3389/fonc.2022.935231.

42 S. M. Pai, P. Chaikin and J. K. Berg, Pharmacokinetics of Lapatinib, a Nonrenally Cleared Drug, in Patients With End-Stage Renal Disease on Maintenance Hemodialysis, *J. Clin. Pharmacol.*, 2019, **59**(10), 1379–1383, DOI: 10.1002/jcph.1430.

43 G. Hannon, F. L. Tansi, I. Hilger and A. Prina-Mello, The Effects of Localized Heat on the Hallmarks of Cancer, *Adv. Ther.*, 2021, **4**(7), 2000267, DOI: **10.1002/adtp.202000267**.

44 W. Zhou, X. Ma, J. Wang, X. Xu, O. Koivisto, J. Feng, T. Viitala and H. Zhang, Co-Delivery CPT and PTX Prodrug with a Photo/Thermo-Responsive Nanoplatform for Triple-Negative Breast Cancer Therapy, *Smart Med.*, 2022, **1**(1), e20220036, DOI: **10.1002/SMMD.20220036**.

45 J. Kolosnjaj-Tabi, I. Marangon, A. Nicolas-Boluda, A. K. A. Silva and F. Gazeau, Nanoparticle-Based Hyperthermia, a Local Treatment Modulating the Tumor Extracellular Matrix, *Pharmacol. Res.*, 2017, **126**, 123–137, DOI: **10.1016/j.phrs.2017.07.010**.

46 X. Li, G. L. Ferrel, M. C. Guerra, T. Hode, J. A. Lunn, O. Adalsteinsson, R. E. Nordquist, H. Liu and W. R. Chen, Preliminary Safety and Efficacy Results of Laser Immunotherapy for the Treatment of Metastatic Breast Cancer Patients, *Photochem. Photobiol. Sci.*, 2011, **10**(5), 817–821, DOI: **10.1039/c0pp00306a**.

47 L. Karthikeyan and R. Vivek, Synergistic Anti-Cancer Effects of NIR-Light Responsive Nanotherapeutics for Chemo-Photothermal Therapy and Photothermal Immunotherapy: A Combined Therapeutic Approach, *Adv. Cancer Biol.: Metastasis*, 2022, **4**, 100044, DOI: **10.1016/j.adcanc.2022.100044**.

48 Y. Tie, F. Tang, Y. Wei and X. Wei, Immunosuppressive Cells in Cancer: Mechanisms and Potential Therapeutic Targets, *J. Hematol. Oncol.*, 2022, **15**(1), 61, DOI: **10.1186/s13045-022-01282-8**.

49 M. Leverkus, Imiquimod: Unexpected Killer, *J. Invest. Dermatol.*, 2004, **122**(5), xv–xvi, DOI: **10.1111/j.0022-202X.2004.22537.x**.

50 A. K. Bubna, Imiquimod - Its Role in the Treatment of Cutaneous Malignancies, *Indian J. Pharmacol.*, 2015, **47**(4), 354–359, DOI: **10.4103/0253-7613.161249**.

51 L. Yang and Y. Zhang, Tumor-Associated Macrophages: From Basic Research to Clinical Application, *J. Hematol. Oncol.*, 2017, **10**(1), 58, DOI: **10.1186/s13045-017-0430-2**.

52 M. Agnoletti, C. Rodríguez-Rodríguez, S. N. Kłodzińska, T. V. F. Esposito, K. Saatchi, H. Mørck Nielsen and U. O. Häfeli, Monosized Polymeric Microspheres Designed for Passive Lung Targeting: Biodistribution and Pharmacokinetics after Intravenous Administration, *ACS Nano*, 2020, **14**(6), 6693–6706, DOI: **10.1021/acsnano.9b09773**.

53 X. Lin, J. He, W. Li, Y. Qi, H. Hu, D. Zhang, F. Xu, X. Chen and M. Zhou, Lung-Targeting Lysostaphin Microspheres for Methicillin-Resistant Staphylococcus Aureus Pneumonia Treatment and Prevention, *ACS Nano*, 2021, **15**(10), 16625–16641, DOI: **10.1021/acsnano.1c06460**.

54 L. Wang, C. Liu, W. Lu, L. Xu, L. Kuang and D. Hua, ROS-Sensitive Crocin-Loaded Chitosan Microspheres for Lung Targeting and Attenuation of Radiation-Induced Lung Injury, *Carbohydr. Polym.*, 2023, **307**, 120628, DOI: **10.1016/j.carbpol.2023.120628**.

55 A. Balfourier, N. Luciani, G. Wang, G. Lelong, O. Ersen, A. Khelfa, D. Alloyeau, F. Gazeau and F. Carn, Unexpected Intracellular Biodegradation and Recrystallization of Gold Nanoparticles, *Proc. Natl. Acad. Sci. U. S. A.*, 2020, **117**(1), 103–113, DOI: **10.1073/pnas.1911734116**.